Springer

Journal of
Mechanical
Science and
Technology

Journal of Mechanical Science and Technology 23 (2009) 2479~2491

www.springerlink.com/content/1738-494x
DOI 10.1007/s12206-009-0707-7

Constrained and non-constrained aerodynamic optimization using the adjoint equations approach †

Mohamad Hamed Hekmat[1,*], Masoud Mirzaei[1] and Ehsan Izadpanah[2]

[1]*Department of Aerospace Engineering, K. N. Toosi University of Technology, Tehran, Iran*
[2]*Department of Mechanical Engineering, Yazd University, Yazd, Iran*

(Manuscript Received January 18, 2009; Revised April 14, 2009; Accepted June 8, 2009)

Abstract

In this research, the continuous adjoint method is applied to optimize an airfoil in subsonic and transonic flows. An inverse design problem is solved to evaluate the ability of the optimization algorithm and then, two types of optimizations, constrained and non-constrained, are investigated in a drag minimization problem. In the non-constrained drag minimization problem, the optimization is performed in a fixed angle of attack with neither geometric nor aerodynamic constraint, but in the constrained drag minimization problem, the optimization is performed in a fixed lift coefficient. Comparison of the results of these two optimizations shows the effects of the constraint on the optimization trend and the optimized geometry. Moreover, imposing the aerodynamic constraint increased the computational costs of the adjoint method. In constrained and non-constrained drag minimization problems, the surface points are adopted as design variables to show the performance of the adjoint equations approach in problems with numerous design variables.

***Keywords*:** Adjoint equations; Constrained optimization; Euler equations; Non-constrained optimization

1. Introduction

Engineers continually strive to improve their designs, both to increase their operational effectiveness and their market appeal. In the design of a complex engineering system, relatively small design changes can sometimes lead to significant benefits. For example, small changes in wing section shapes can lead to large reduction in shock strength in transonic flow. Changes of this type are unlikely to be discovered by trial and error methods, and for such situations that optimization methods can play an important role.

In the past for a suitable design that provides a desired aerodynamic performance, designers needed to build numerous models for wind tunnel testing to confirm the final design performance. Such a design process does not allow for vast numbers of design iterations or variables to be considered. The development of computational fluid dynamics during recent decades has made it possible to evaluate alternative designs by numerical simulation. The use of computational simulation to scan many alternative designs has proved extremely valuable in practice, but it still suffers a limitation finding the best possible design. To ensure the recognition of the true best design, the ultimate goal of computational simulation methods should not just be the analysis of prescribed shapes, but automatic determination of the true optimum shape for the desired application. This is the underlying motivation for the combination of computational fluid dynamics with numerical optimization methods.

The adjoint method is a gradient-based method which has been used extensively in many aerodynamic optimization problems in recent decades. In fluid dynamics, the first use of adjoint equations method for design purpose was reported by Piron-

† This paper was recommended for publication in revised form by Associate Editor Yang Na

*Corresponding author. Tel.: +98 2177791044, Fax.: +98 2177791045
E-mail address: mhamed_hekmat@yahoo.com

neau [1], but this method for optimal aerodynamic design was first applied to transonic flow by Jameson [2-4]. He formulated the method for inviscid compressible flows with shock waves governed by both the potential flow and the Euler equations. Elliot and Peraire [5] used the discrete adjoint method on unstructured meshes for the inverse design of airfoils and in transonic flow to produce specified pressure distributions. In [6], Dadone and Grossman explored the discrete adjoint method and applied it in the progressive optimization strategy. A comparison of both continuous and discrete adjoint approaches was conducted by Nadarajah and Jameson [7-9]. Baysal and Ghayour [10] derived the adjoint equations in Cartesian coordinates on an unstructured grid system using Roe scheme. Vitturia and Beux [11] implement the discrete adjoint approach for aerodynamic optimization in a turbulent viscous flow. The adjoint method has also been used by many researchers in aerodynamic optimization including Xie [12], Qiao et al. [13], Gauger and Brezillon [14], Dwight and Brezillon [15], Amoignon [16] and Hazra [17].

The objective of the present paper is to implement the adjoint approach for airfoils optimization in constrained and non-constrained drag minimization problems. First, an inverse design problem is solved to evaluate the optimization algorithm. Then, the drag minimization problem is investigated as a constrained and a non-constrained problem to show the effect of aerodynamic constraint on the optimization results. It was shown that the mechanism, value and the trend of drag reduction and shape variations during the optimization process were strongly affected by the aerodynamic constraint.

2. General description of the adjoint method

For flow over an airfoil or wing, the aerodynamic properties which define the cost function (I) are dependent on the flow field variables (w) and the physical location of the boundary, which may be represented by the function F:

$$I = I(w, F) \tag{1}$$

Since w depends on F, a change in F changes the cost function as:

$$\delta I = \left[\frac{\partial I^T}{\partial w}\right]_I \delta w + \left[\frac{\partial I^T}{\partial F}\right]_{II} \delta F \tag{2}$$

The first term is the contribution due to the variation δw in the flow field and the second term is the direct effect of the geometry change. Assume R is the governing equation which expresses the relation of w and F in the flow field domain D:

$$R(w, F) = 0 \tag{3}$$

Then δw is determined from the equation:

$$\delta I = \left[\frac{\partial I^T}{\partial w}\right]_I \delta w + \left[\frac{\partial I^T}{\partial F}\right]_{II} \delta F \tag{4}$$

Since the variation δR is zero, it can be multiplied by a Lagrange multiplier ψ and subtracted from the variation δI with no change in the result. Thus Eq. (2) can be replaced by:

$$\begin{aligned} &\delta I = \\ &\frac{\partial I}{\partial w}^T \delta w + \frac{\partial I}{\partial F}^T \delta F - \psi^T \left(\left[\frac{\partial R}{\partial w}\right]\delta w + \left[\frac{\partial R}{\partial F}\right]\delta F\right) \\ &= \left\{\frac{\partial I}{\partial w}^T - \psi^T \left[\frac{\partial R}{\partial w}\right]\right\}\delta w + \left\{\frac{\partial I}{\partial F}^T - \psi^T \left[\frac{\partial R}{\partial F}\right]\right\}\delta F \end{aligned} \tag{5}$$

To eliminate the dependence of δI to δw, ψ must satisfy the adjoint equations:

$$\left[\frac{\partial R}{\partial w}\right]^T \psi = \frac{\partial I}{\partial w} \tag{6}$$

The first term is eliminated, and we find that:

$$\delta I = G \delta F \tag{7}$$

where

$$G = \frac{\partial I}{\partial F}^T - \psi^T \left[\frac{\partial R}{\partial F}\right] \tag{8}$$

According to Eq. (7) and (8), δI is independent of δw and, as a result, for a large number of design variables we can compute the gradient vector (G) only with one flow solution in addition to one adjoint solution in each design cycle. In fact, the computational cost of the adjoint equations solution is independent of the number of design variables. It should be noted that the computational cost of one adjoint solution is less than one flow solution. After calculating the gradient vector, we can improve the design variables using an optimization algorithm such as steepest de-

scent method or smoothed steepest descent algorithm.

3. Governing equations

In this study the Euler equations are the governing equations of the flow field. The conservative form of two-dimensional Euler equations is:

$$\frac{\partial w}{\partial t}+\frac{\partial f_i}{\partial x_i}=0 \tag{9}$$

where w is flow variables and f_i is the inviscid flux vector:

$$w=\begin{bmatrix}\rho\\ \rho u_1\\ \rho u_2\\ \rho E\end{bmatrix},\ f_i=\begin{bmatrix}\rho u_i\\ \rho u_i u_1+\delta_{i1}p\\ \rho u_i u_2+\delta_{i2}p\\ \rho u_i H\end{bmatrix} \tag{10}$$

and δ_{ij} is the Kronecker delta function and:

$$p=(\gamma-1)\rho\left\{E-\frac{1}{2}(u_i^2)\right\} \tag{11}$$

$$\rho H=\rho E+p \tag{12}$$

In these definitions, ρ is the density, E is total energy, H is total enthalpy and γ is the ratio of specific heats.

Using a transformation from physical coordinates to computational coordinates, the Euler equations can be written as:

$$\frac{\partial W}{\partial t}+R(W)=0 \tag{13}$$

where

$$R(W)=\frac{\partial F_i}{\partial \xi_i},\ W=Jw,$$
$$F_i=S_{ij}f_j=\begin{bmatrix}\rho U_i\\ \rho U_i u_1+S_{i1}p\\ \rho U_i u_2+S_{i2}p\\ \rho U_i H\end{bmatrix} \tag{14}$$

and

$$K_{ij}=\begin{bmatrix}\frac{\partial x_i}{\partial \xi_j}\end{bmatrix},\ J=\det(K),\ S=JK^{-1} \tag{15}$$

The scaled contravariant velocity components are introduced as:

$$U_i=S_{ij}u_j \tag{16}$$

In the computational domain, airfoil surface B_W is presented by $\xi_2=0$. The boundary condition on the airfoil surface is:

$$U_2=0 \tag{17}$$

On the far field boundary, the free stream condition is applied.

A finite-volume technique with an artificial dissipation method introduced by Jameson et al. [18] is used to discrete the integral form of the conservation equations. For temporal approximation, we applied the five stage modified Runge-Kutta approach. Since the time step in explicit methods is small, we implemented the convergence acceleration techniques, local time stepping and residual averaging, to accelerate the convergence rate.

4. Adjoint equations

The adjoint equations can be obtained:

$$\frac{\partial \psi}{\partial t}-C_i^T\frac{\partial \psi}{\partial \xi_i}=0 \tag{18}$$

where ψ is adjoint variables vector and:

$$C_i=S_{ij}A_j,\ A_j=\frac{\partial f_j}{\partial w} \tag{19}$$

The adjoint boundary conditions on the surface can be derived as follows:

$$\begin{aligned}
&\psi_{1_{i,1}}=\psi_{1_{i,2}}\\
&\psi_{2_{i,1}}=\psi_{2_{i,2}}+2n_1(\lambda-n_1\psi_{2_{i,2}}-n_2\psi_{3_{i,2}})\\
&\psi_{3_{i,1}}=\psi_{3_{i,2}}+2n_2(\lambda-n_1\psi_{2_{i,2}}-n_2\psi_{3_{i,2}})\\
&\psi_{4_{i,1}}=\psi_{4_{i,2}}
\end{aligned} \tag{20}$$

For the inverse design problem:

$$\lambda=p-p_d \tag{21}$$

and for the constrained drag minimization problem:

$$\lambda=\frac{-2}{\gamma p_\infty M^2{}_\infty c}\big[\ (n_1\cos\alpha+n_2\sin\alpha)+\Phi(n_2\cos\alpha-n_1\sin\alpha)\ \big] \tag{22}$$

where

$$\Phi = -\frac{\dfrac{\partial C_d}{\partial \alpha}}{\dfrac{\partial C_l}{\partial \alpha}} \tag{23}$$

In the above relations, p_d is the desired pressure in the inverse design, p_∞ and M_∞ are the free stream pressure and Mach number, c is chord length, α is angle of attack, C_l is lift coefficient and n_i are the components of unit vector normal to the surface where can be derived as follows:

$$n_i = \frac{S_{2i}}{\sqrt{S_{2j}\, S_{2j}}} \tag{24}$$

The subscripts (i,1) and (i,2) in the above equations denote cells below and above the wall. For $\Phi = 0$ in Eq. (22), the adjoint boundary condition on the surface of the airfoil is obtained for a non-constrained problem. For subsonic and transonic flows that the outer boundary is far from the body, we can set

$$\psi_{1-4} = 0 \tag{25}$$

Because of the similarity of the adjoint equations to the flow equations, the same numerical methods applied for solution of the flow equations can be used to solve the adjoint equations.

5. Constrained optimization

In the drag minimization problem, we want to maintain the lift coefficient constant and equal to its initial value by changing the angle of attack. Therefore, in this case:

$$\delta I = \delta C_d = \frac{\partial C_d}{\partial w}\delta w + \frac{\partial C_d}{\partial F}\delta F + \frac{\partial C_d}{\partial \alpha}\delta \alpha \tag{26}$$

and the additional constraint is:

$$\delta C_l = \frac{\partial C_l}{\partial w}\delta w + \frac{\partial C_l}{\partial F}\delta F + \frac{\partial C_l}{\partial \alpha}\delta \alpha = 0 \tag{27}$$

or

$$\delta \alpha = -\frac{\dfrac{\partial C_l}{\partial w}\delta w + \dfrac{\partial C_l}{\partial F}\delta F}{\dfrac{\partial C_l}{\partial \alpha}} \tag{28}$$

The angle of attack is updated by using Eq. (28) in each design cycle. To compute $\delta\alpha$, an additional adjoint equation needs to be solved.

6. Cost function and design variables

The choice of design variables is one of the most crucial steps in any optimization procedure. In fact, the success of an optimization method strongly depends on both the choice of design variables and the cost function.

The cost function for the inverse design problem in computational domain is defined as:

$$I = \frac{1}{2}\int_{Bw} (p - p_d)^2 \, |ds| \, d\xi \tag{29}$$

Where

$$|ds| = \sqrt{S_{2j}\, S_{2j}} \tag{30}$$

and the cost function for the drag minimization problem is defined as:

$$C_d = \frac{-2}{\gamma\, p_\infty M_\infty^2 c}\int_{Bw} p\,(S_{21}\cos\alpha + S_{22}\sin\alpha)\, d\xi \tag{31}$$

In the present work two approaches of parameterizing the airfoil surface are used. One approach employs the surface grid points and the other one uses the definition of the NACA 4-digit airfoil series. The use of the surface grid points as design variables ensures that there is no restriction on the attainable geometry. Since the cost of the adjoint approach is independent of the number of design variables, it is feasible to use the surface points as design variables, whereas the cost would be prohibitive if the gradients were computed by the traditional finite-difference method. In this case, design variables are y components of grid points on the surface. In NACA 4-digit airfoil series, three parameters, m (the maximum mean camber), p (the chordwise position of the maximum mean camber) and t (maximum thickness of the airfoil) are used to define the airfoil shape. Here m, t are taken as design variables and p is assumed to be 0.4.

7. Optimization algorithm

After calculation of the gradient vector, we can change the values of the design variables using an optimization algorithm. Steepest descent algorithm

and smoothed steepest descent algorithm have been adapted to treat the design variables towards optimum values. In the steepest descent algorithm, the design variable vector x can be updated as:

$$x^{n+1} - x^n = -\alpha \nabla f \tag{32}$$

where α is the step length and ∇f is gradient vector of the cost function. In the smoothed steepest descent algorithm, the design variable vector x can be updated as:

$$\delta x = -\alpha \bar{\nabla} f \tag{33}$$

We replace the gradient ∇f by a smoothed gradient $\bar{\nabla} f$. To apply smoothing in the x direction, the smoothed gradient $\bar{\nabla} f$ may be calculated by a discrete approximation such as:

$$\bar{\nabla} f - \frac{\partial}{\partial \xi} \varepsilon \frac{\partial}{\partial \xi} \bar{\nabla} f = \nabla f \tag{34}$$

where ε is the smoothing parameter. Jameson and Vassberg [19] show that the implicit smoothing technique corresponds to an implicit time stepping scheme for the descent equation:

$$\frac{\partial x}{\partial t} = -\nabla f \quad (in\ \alpha \to 0) \tag{35}$$

if the smoothing parameter is chosen appropriately.

The smoothing ensures that each new shape in the optimization process remains smooth. Consequently, it is necessary to smooth the gradient vector when we apply surface points as design variables. The smoothing also allows us to use much larger steps, and leads to a large reduction in the number of design iterations.

8. Grid modification

Jameson [2, 4] introduced a method that modifies the current location of the grid points based on perturbations at the surface geometry. This method was also successfully used by Burgreen et al. [20]. In this method, the grid points are modified along each grid index line projecting from the surface. At first, the arc length between the surface point and the far-field point along the grid line is computed and then the grid points at each location along the grid line are attenuated proportional to its arc length distance from the surface point and the total arc length between the surface and the far-field. The algorithm can be as:

$$\begin{cases} x_{i,j}^{new} = x_{i,j}^{old} + C_j \left(x_{i,1}^{new} - x_{i,1}^{old} \right) \\ \qquad\qquad\qquad\qquad j = 2, \ldots, j_{\max} \\ y_{i,j}^{new} = y_{i,j}^{old} + C_j \left(y_{i,1}^{new} - y_{i,1}^{old} \right) \end{cases} \tag{36}$$

where i is the current grid index and:

$$C_j = 1 - (3 - 2N_j) N_j^2 \tag{37}$$

N is the ratio of the arc length from the surface to the current grid point and the total arc length from the surface to the far-field along the grid line:

$$N_j = \frac{\sum_{\ell=2}^{j} \sqrt{(x_{i,\ell} - x_{i,\ell-1})^2 + (y_{i,\ell} - y_{i,\ell-1})^2}}{\sum_{\ell=2}^{j_{\max}} \sqrt{(x_{i,\ell} - x_{i,\ell-1})^2 + (y_{i,\ell} - y_{i,\ell-1})^2}} \tag{38}$$

Fig. 1 represents the performance of the method.

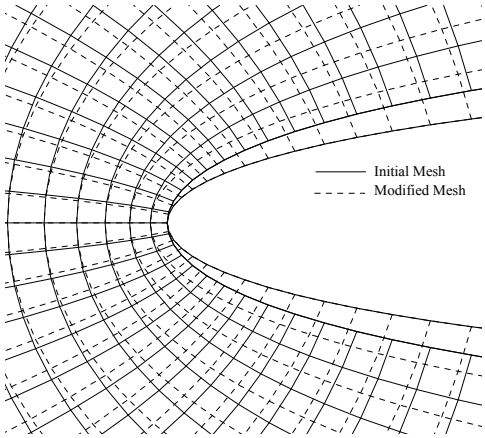

Fig. 1. Example of the Jameson grid modification method.

9. Optimization results

Finally, the design procedure using the adjoint method can be summarized as Fig. 2.

Since the flow field solution performs a major role in evaluation of the cost function, the accuracy of the flow field solver should be validated. The results of the present solver are compared with those of [21]. Fig. 3 gives the pressure coefficient of NACA 0012 airfoil for free stream conditions of M=0.8 and α=1.25 degrees. It can be seen that the present results are in good agreement with the experimental data.

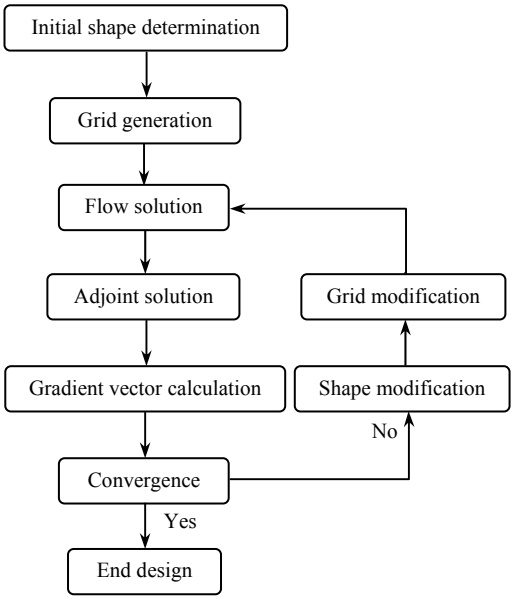

Fig. 2. Design cycle.

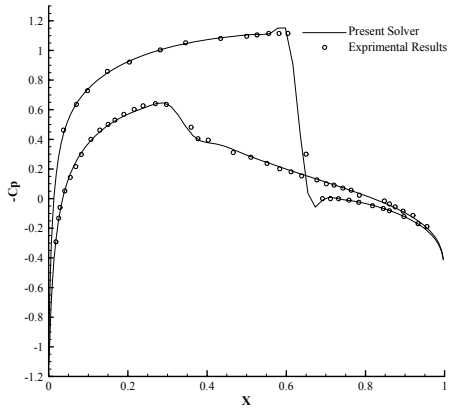

Fig. 3. Comparison of experimental pressure coefficient [21] and calculated pressure coefficient by present solver in M=0.8 and α=1.25 degrees.

9.1 Inverse pressure design problem

In this test case, NACA2415 is designed from NACA0012 airfoil. The flow is subsonic with Mach number of 0.65. Both the initial and target airfoils are at zero degree angle of attack. Airfoil camber (m) and its thickness (t) are used as the design variables. A 160×80 cells O-Type grid is employed in this calculation. The convergence criteria for flow governing equations and for adjoint equations were considered as 10^{-8} and 10^{-4} respectively. The initial values for m and t are 0.00, 0.12 and the target values are 0.02, 0.15, respectively.

Table 1. Design results.

	m	t	I	$\|G\|$
Initial	0.0000	0.1200	5.84E-3	4. 35E-1
Optimal	0.02003	0.15005	8.80E-6	3.30E-4

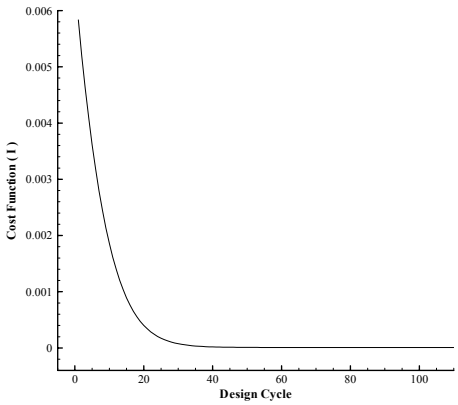

Fig. 4. Convergence history of the cost function for the inverse design problem.

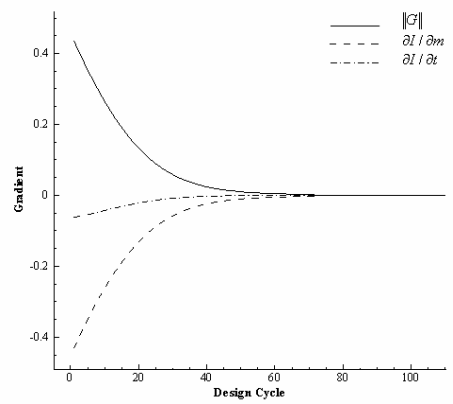

Fig. 5. Convergence history of the norm of the gradient vector and its components for the inverse design problem.

Table 1 presents the design results. The optimal values for t and m are very close to the target values. It should be noted that convergence of the gradient vector norm was considered as the convergence criterion of the optimization program. Fig. 4 shows the convergence history of the cost function. The main variations of the cost function approximately occur during 40 initial cycles, and after 70 cycles the convergence rate approaches to zero. The final design is obtained after 110 cycles. Fig. 5 shows the convergence history of the gradient during the design process. It can be seen

Table 2. Comparison of the adjoint and the finite difference methods.

	$\partial I / \partial m$	$\partial I / \partial t$
Adjoint method	-0.4308	-0.0616
Finite difference method	-0.4317	-0.0609

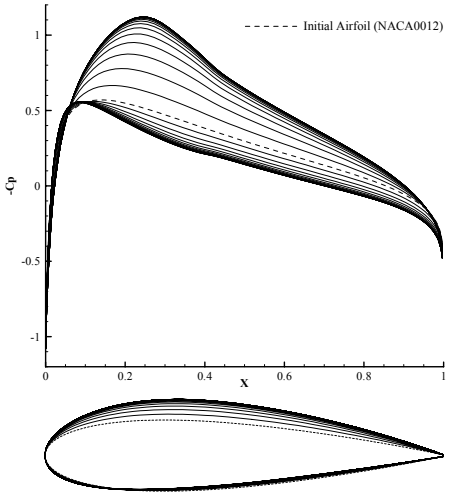

Fig. 6. Variations of pressure distribution and airfoil shape in the inverse design problem.

that the trend is similar to that of the cost function. Fig. 6 shows variations of the pressure coefficient and the shape during the design process. It can be seen that the pressure distribution approaches to that of NACA2415.

It should be noted that the convergence rate of the optimization program is strongly dependent on the step size of α in optimization algorithm. If the step size was taken larger, it increased the convergence rate. But adoption of a larger step size for α leads to decrease in accuracy of the calculated gradients. Sometimes a larger step size caused oscillatory behavior of the gradients. Moreover, adoption of a smaller step size for α led to an increase in the number of design cycles. To validate the adjoint method, the gradients of the cost function of the adjoint method were compared with those of the finite difference method. Table 2 gives this comparison. Good conformity can be seen between the results of these two methods.

The results of the inverse design problem confirm the robustness of the algorithm.

9.2 Drag minimization problem

To evaluate the performance of the adjoint method in design problems with design constraints and also to evaluate the effects of these constraints on the optimization results, two types of optimizations, constrained and non-constrained, are investigated. In both of these types the surface points are used as the design variables. The design is started with an NACA64A410 airfoil at -0.34 degrees angle of attack. The flow is transonic with Mach number of 0.75. We performed computations on a 160×80 O-grid. The convergence criteria for flow governing equations and for adjoint equations were considered 10^{-8} and 10^{-4} respectively.

Table 3. Design results.

	C_d	C_l	α
Initial	0.0146	0.5693	-0.34
Optimal	0.00199	0.2943	-0.34

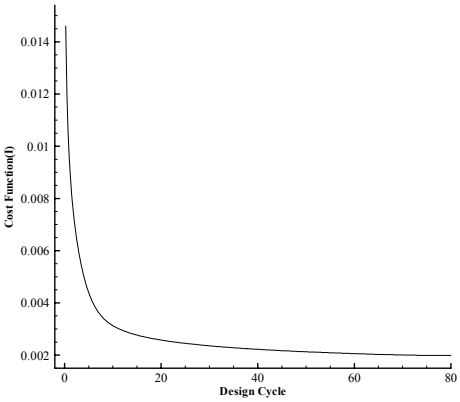

Fig. 7. Convergence history of the cost function for the non-constrained drag minimization problem.

9.3 Non-constrained drag minimization

In this case, the optimization is performed in a fixed angle of attack with no aerodynamic constraints.

Table 3 represents the design results. We obtained 86.37 percent reduction in drag coefficient. Fig. 7 represents the convergence of the cost function. This figure shows that full convergence of aerodynamic optimization is obtained after 80 design iterations. After four design cycles, 55.67 percent reduction in drag coefficient was obtained. Note that the 40 final cycles obtained only 1.79 percent reduction. Fig. 8 shows the gradient of the cost function of each design variable at the initial and final design cycle. According to this figure, sensitivity of the cost function to the

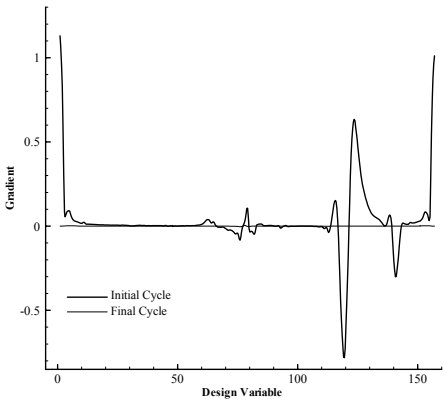

Fig. 8. Initial and final gradients of the cost function for the non-constrained drag minimization problem.

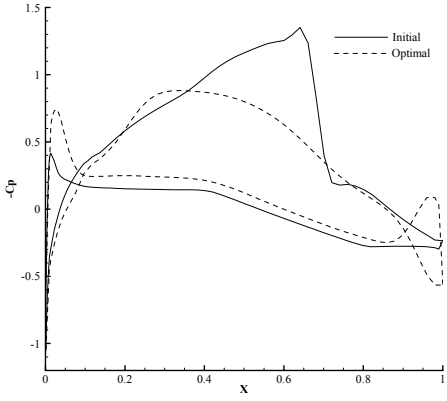

Fig. 9. Comparison of pressure coefficient of NACA64A410 and optimal airfoils for the non-constrained drag minimization problem.

upper surface points at the region where the shock wave occurs and at the trailing edge region is higher than that of the other points.

Fig. 9 represents the initial and optimal pressure coefficient. The figure shows that the shock on the initial airfoil surface has been weakened strongly and drag has been reduced, but also the surface area under the curve which represents the value of the lift, has been reduced. Fig. 10 shows the geometry of initial and optimized airfoils. The change in geometry at the upper surface and around the trailing edge is considerable, whereas this change at the lower surface is very small. Fig. 9 and 10 show that the upper surface of the optimized airfoil has approached to a flat geometry. The flat surface has weakened the shock. Further more, the geometry of the trailing edge has curved to upward. This causes reduction in the drag. Fig. 11 shows the

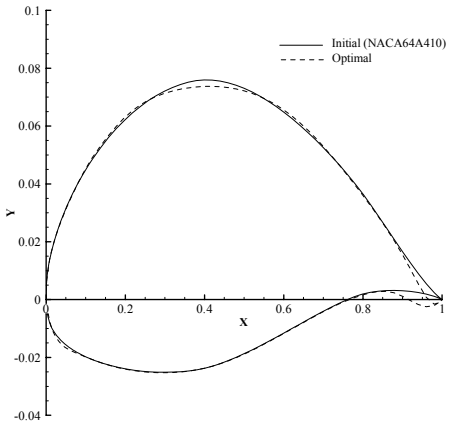

Fig. 10. Comparison of NACA64A410 airfoil and optimal airfoil geometries for the non-constrained drag minimization problem.

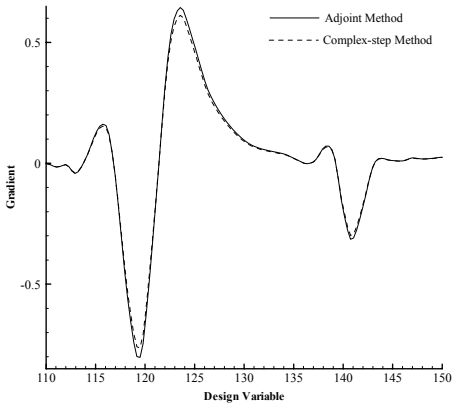

Fig. 11. Adjoint versus complex-step gradients for the non-constrained drag minimization problem.

initial gradients of the adjoint and complex-step methods. Lyness [22] introduced the complex-step in calculating the derivative of an analytical function.

Fig. 12 compares the initial and optimal pressure contours. The figure shows that the strength of shock wave on the initial airfoil surface has been weakened.

9.4 Constrained drag minimization

In this case, the optimization is performed in a fixed lift and angle of attack is applied as an additional design variable to fix lift during the design process.

Table 4 represents the design results. The reduction in the drag coefficient is considerable. We obtained 78.21 percent reduction in drag coefficient, but the variation of the lift coefficient is very small (2.3 percents). Fig. 13 gives the variation of the cost function

Table 4. Design results.

	C_d	C_l	α
Initial	0.0146	0.5693	-0.34
Optimal	0.00318	0.5561	-1.23

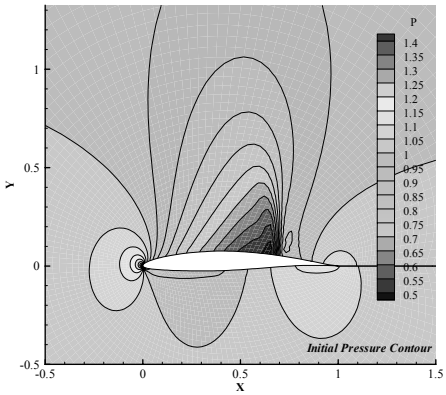

(a)

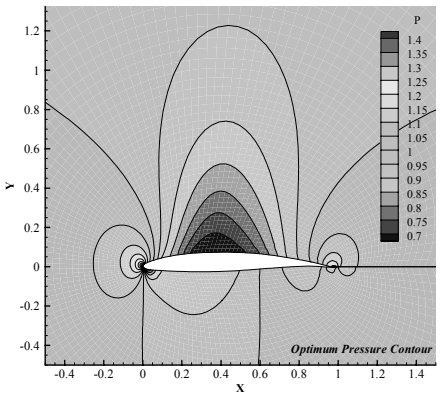

(b)

Fig. 12. Pressure contours for the non-constrained drag minimization problem. (a) Initial and (b) optimal

with design cycle. For this problem, the design cycle has 90 iterations. According to this figure, the convergence rate is very sharp at initial cycles. The drag coefficient reduction is 76.44 percent during the first 50 design cycles. This coefficient has only 1.77 percent reduction the last 40 cycles. Fig. 14 represents the initial and final gradient of the cost function (drag coefficient) for the constrained design minimization problem. The value of gradients of cost function with respect to design variables is considerable in the initial cycle, but the gradients reach to zero at the end of the design process. Sensitivity of the cost function on upper surface points and area near the trailing edge is

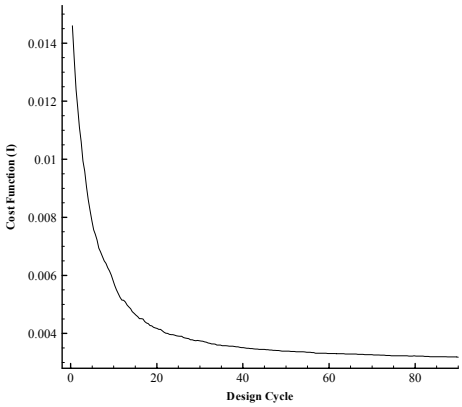

Fig. 13. Convergence history of the cost function for the constrained drag minimization problem.

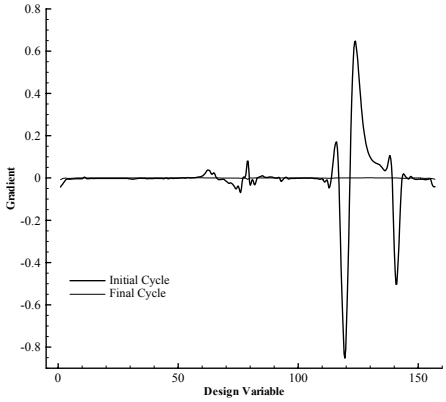

Fig. 14. Initial and final gradients of the cost function for the constrained drag minimization problem.

more than other surface points. According to Figs. 13 and 14, the convergence of the optimization program is evident.

Fig. 15 represents the initial and optimal pressure coefficients. The figure shows that the strong shock on the initial airfoil surface has been weakened strongly and drag coefficient has been reduced, but the surface area under the curve, which represents the value of the lift coefficient, has remained constant; consequently, this coefficient is nearly the same for both the initial and optimal airfoils. Fig. 16 shows the geometry of initial and optimal airfoils. Figs. 15 and 16 show that the upper surface of the optimal airfoil has approached to a flat geometry. The flat surface has weakened the strength of the shock wave. Furthermore, the geometry of at its trailing edge has curved downward to compensate the reduction of the lift due to the weakening the strength of the shock.

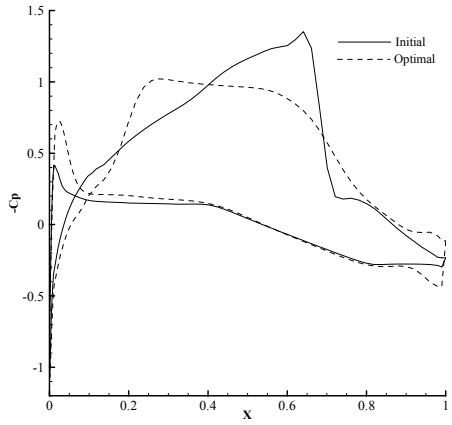

Fig. 15. Comparison of pressure coefficient of NACA64A10 and optimal airfoils for the constrained drag minimization problem.

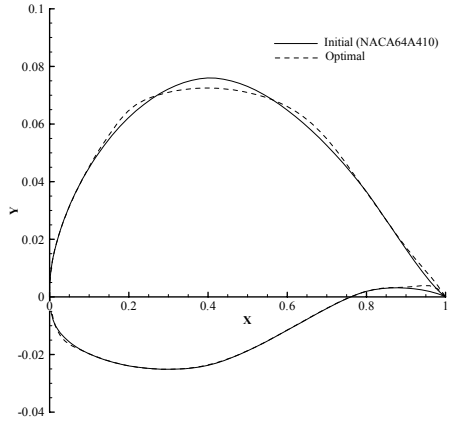

Fig. 16. Comparison of NACA64A410 airfoil and optimal airfoil for the constrained drag minimization problem.

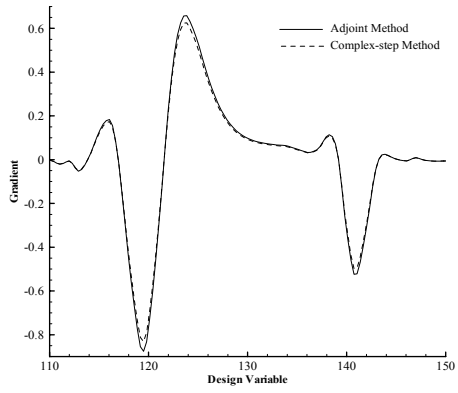

Fig. 17. Adjoint versus complex-step gradients for the constrained drag minimization problem.

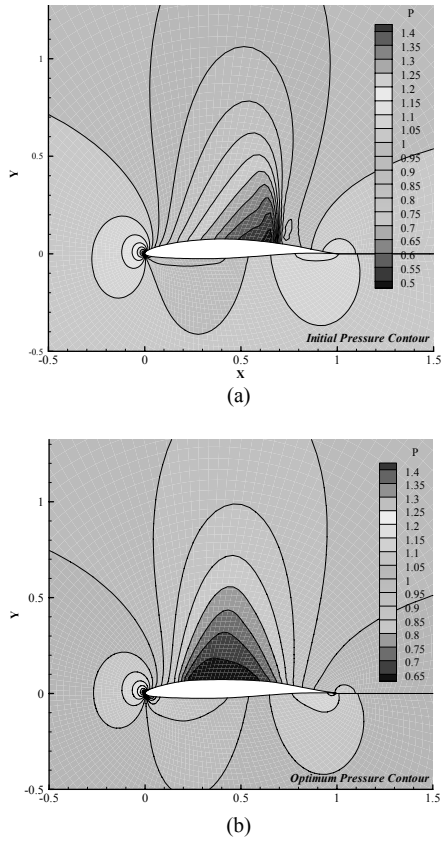

Fig. 18. Pressure contours for the constrained drag minimization problem. (a) Initial and (b) optimal

Fig. 17 shows the values of the initial gradients obtained from the adjoint and complex-step methods at the surface points of NACA64A410 airfoil. Fig. 18 compares the initial and optimal pressure contours.

9.5 Validation of the optimization results

To assure the validation of the results, it is necessary to investigate the validation of the obtained gradients. (In this study, the gradients of the cost function of the adjoint method were compared with those of the finite difference method (in inverse design problem) and complex-step method (in drag minimization problem)). In most studies of adjoint method, the accuracy of the inverse design problem results has been used to validate the optimization results, which also in this study, the accuracy of inverse design results confirms the validation of obtained optimization results.

However, we compared the constrained optimization results with results of [23] in the same initial conditions of grid and flow field (NACA64A410

Table 5. Comparison of the obtained optimal aerodynamic coefficients of the present study with results of [23] in the constrained drag minimization problem.

		C_l	C_d
Present results	Initial	0.5693	0.0146
	Optimal	0.5561	0.00318
Results of reference [23]	Initial	0.5684	0.0140
	Optimal	0.5568	0.00324

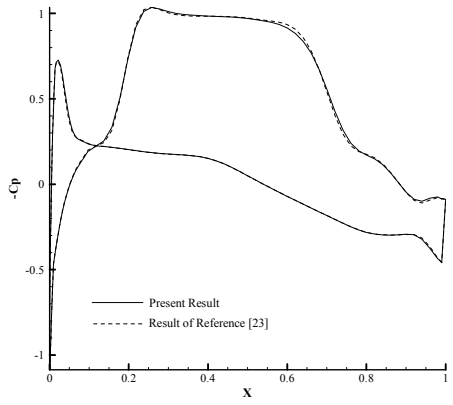

Fig. 19. Comparison of the obtained optimal pressure distribution of the present study with the obtained optimal pressure distribution of [23] in the constrained drag minimization problem.

airfoil at -0.34 degrees angle of attack, mach number of 0.75 and 160×80 O-grid). Table 5 and Fig. 19 compare the obtained optimal results of the present study with the obtained optimal results of [23] in the constrained drag minimization problem. Good conformity can be seen between our results and [23].

9.6 Comparison of the constrained and non-constrained optimization results

The adjoint method is a gradient-based method, and according to the optimization algorithm in this study, it is expected that the adjoint method conducts the optimization process in a way that the most variations occur in some areas of the body in which gradients of cost function have larger values. In Fig. 8 and Fig. 14, there are some cases in which that can be seen obviously. Sensitivity of the cost function on upper surface points (the place that shock waves take place) and area near the trailing edge is more than other surface points, and it is believed that most variations of geometry should happen in these areas. The objective

Table 6. Runtime and number of adjoint and flow solvers.

	Runtime	Number of adjoint solvers	Number of flow solvers	Number of design cycles
Non-constrained drag minimization problem	3 hrs 18 mins	80	80	80
Constrained drag minimization problem	8 hrs 25mins	180	90	90

in the non-constrained optimization problem is drag reduction only and no geometry or aerodynamic constraint is applied. Therefore, it is logical that the optimization algorithm conducts the optimization process towards reaching this objective. In this case, the used optimization algorithm performs drag reduction by means of reduction of shock wave strength on the upper surface using flattening of the surface in that area and curving upward the trailing edge geometry (Fig. 9 and Fig. 10). Nowadays, these two drag reduction mechanisms are widely used in practice. For example, in designing supercritical airfoils in order to minimize drag, flattening the upper surface has been used, or in air vehicles, the variations of trailing edge curvature of the wing are utilized to control and direct the vehicle. So, the obtained optimization results agree with facts and considerations which are used in designs, but in this study we obtained these facts using an optimization method. But the objective in a constrained drag minimization problem is drag reduction and keeping lift constant. Drag reduction is performed by means of reduction of shock wave strength on the upper surface using flattening of the upper surface (Fig. 15), but this drag reduction leads to lift reduction, and therefore it is expected that in the trailing edge, the optimization algorithm acts (opposite the non-constrained problem) in a manner that the geometry variations in this area do not lead to more lift reduction and compensate lift reduction generated by drag reduction (according to Fig. 16 the curvature of trailing edge is downward (against the previous case (Fig. 10)). This is exactly the same as considerations used in designing supercritical airfoils (flattening the upper surface to reduce drag and curving the geometry of trailing edge downward to compensate lift reduction generated by drag reduction).

As stated previously in the constrained problem, the angle of attack should be changed to set the lift at

a constant value at each design cycle. To calculate the variation of the angle of attack at each design cycle, Eq. (28) is used. In this equation, the nominator of the right side term is the same as that of the lift coefficient variation, so to calculate $\delta\alpha$, first δC_l should be calculated. Consequently, the adjoint equations should be solved again. In fact, adding the constant lift coefficient constraint increases the computational costs. Table 6 summarizes the required runtime and number of adjoint and flow solvers to achieve the convergence of the optimization program for the drag minimization problem. The results show that constrained optimization takes more computational time.

10. Conclusions

In this paper, the adjoint approach is implemented for an inverse pressure design and a drag minimization problem with and without lift constraint. In the inverse design problem, values of camber and thickness (design variables) were obtained successfully. In the non-constrained drag minimization problem, the optimization is performed with no aerodynamic constraints, but in the constrained drag minimization problem, the optimization is performed in a fixed lift and angle of attack is applied as an additional design variable to fix lift during the design process. Comparison of the results of these optimizations shows that the mechanism, value, the trend of drag reduction during the optimization process and the optimized geometry is strongly affected by the applied constraint. In the constrained drag minimization problem, an extra adjoint equation should be solved for each constant in each design cycle and more computational efforts are needed. It is concluded that using this approach for optimization problems with numerous constraints is not efficient. To evaluate the performance of the adjoint method in design problems with numerous design variables, the surface points of the airfoils are adopted as design variables in the drag minimization problem.

References

[1] O. Pironneau, On optimal profiles in Stokes flow, *J. Fluid Mech.*, 59 (1) (1973) 117-128.

[2] A. Jameson, Aerodynamic design via control theory, *J. of Scientific Computing*, 3 (3) (1988) 233-260.

[3] A. Jameson and J. J. Alonso, Automatic aerodynamic optimization on distributed memory architectures, AIAA paper 96-0409, *34th Aerospace Sciences Meeting and Exhibit*, Reno, Nevada, USA, (1996).

[4] A. Jameson, Re-engineering the design process through computation, AIAA paper 97-0641, *35th Aerospace Sciences Meeting and Exhibit*, Reno, Nevada, USA, (1997).

[5] J. Elliott and J. Peraire, 3-D aerodynamic optimization on unstructured meshes with viscous effects, AIAA paper 97-1849, *35th Aerospace Sciences Meeting and Exhibit*, Reno, Nevada, USA, (1997).

[6] A. Dadone and B. Grossman, Progressive optimization of inverse fluid dynamic design problems, *J. Computers & Fluids*, 29 (3) (2000) 1-32.

[7] S. Nadarajah and A. Jameson, A comparison of the continuous and discrete adjoint approach to automatic aerodynamic optimization, AIAA paper 2000-0667, *38th Aerospace Sciences Meeting and Exhibit*, Reno, Nevada, USA, (2002).

[8] S. Nadarajah and A. Jameson, Studies of the continuous and discrete adjoint approaches to viscous automatic aerodynamic shape optimization, AIAA paper 2001-2530, *15th. Computational Fluid Dynamics Conference*, Anaheim, USA, (2001).

[9] S. Nadarajah, *The Discrete Adjoint Approach to Aerodynamic Shape Optimization*, Ph.D. Thesis, Stanford University, Stanford, USA, (2003).

[10] O. Baysal and K. Ghayour, Continuous adjoint sensitivities for optimization with general cost functional on unstructured meshes, *J. AIAA*, 39 (1) (2001) 48-55.

[11] M. Michieli Vitturia and M. F. Beux, A discrete gradient-based approach for aerodynamic shape optimization in turbulent viscous flow, *J. Finite Elements in Analysis and Design*, 5 (12) (2006) 16-23.

[12] L. Xie, *Gradient-Based Optimum Aerodynamic Design Using Adjoint Methods*, Ph.D. Thesis, Virginia Polytechnic Institute and State University, USA, (2002).

[13] Z. D. Qiao, X. D. Yang, X. L. Qin and B. Zhu, Numerical optimization design by solving adjoint equations, *ICAS Congress*, (2002).

[14] N. R. Gauger and J. Brezillon, Aerodynamic shape optimization using adjoint method, *J. Aero. Soc. of India*, 54 (3) (2002) 110-118.

[15] R. P. Dwight and J. Brezillon, Effect of various approximations of the discrete adjoint on gradient-based optimization, *44th AIAA Aerospace Sciences Meeting and Exhibit Conference*, Reno, Nevada, USA, (2006).

[16]O. Amoignon, *Adjoint-Based Aerodynamic Shape Optimization*, Ph.D. Thesis, Uppsala University, Sweden, (2004).
[17]S. B. Hazra, An efficient method for aerodynamic shape optimization, *10th AIAA/ISSMO Multidisciplinary Analysis and Optimization Conference*, New York, USA, (2004).
[18]A. Jameson, W. Schmidt and E. Turkel, Numerical solutions of the Euler equations by finite volume methods with Runge-Kutta time stepping schemes, AIAA paper 81-1259, (1981).
[19]A. Jameson and J. C. Vassberg, Studies of alternative numerical optimization methods applied to the brachistochrone problem, *OptiCON 99*, (1999).
[20]G. W. Burgreen and O. Baysal, Three-dimensional aerodynamic shape optimization of wings using sensitivity analysis, AIAA paper 94-0094, *32nd Aerospace Sciences Meeting and Exhibit*, Reno, Nevada, USA, (1994).
[21]Http://xoptimum.narod.ru/results/compressible/NACA0012.
[22]J. N. Lyness and C. B. Moler, Numerical differentiation of analytic functions, *SIAM Journal on Numerical Analysis*, 4 (2) (1967) 202–210.
[23]S. P. Pournaderi and A. R. Pishevar, Aerodynamic shape optimization using the adjoint approach, *J. of Computational and Applied Mechanics*, 17 (4) (2005) 96-104.

Mohamad Hamed Hekmat received his B.S. in Mechanical Engineering from Yazd University, Iran in 2004. He then received his M.S. in Aerospace Engineering from K. N. Toosi university of Technology Tehran, Iran in 2008. His research interests include fluid mechanics, CFD, aerodynamics and heat transfer.

Masoud Mirzaei received B.S. degree in Mechanical Engineering from Isfahan University of technology, Iran in 1989. He then received his M.S. degree in Thermal Fluid Engineering from Amirkabir University of Technology in 1992. In 1994, he was accepted as a Ph.D. student in Tarbiat Modarres University, Iran, and graduated in 1999. He was employed by K. N. Toosi University of Technology in 2000 as faculty member of aerospace department. His research interests include fluid mechanics, aerodynamics, CFD, and heat transfer.

Ehsan Izadpanah received his B.S. and M.S. degrees in Mechanical Engineering from Yazd University, Iran in 2004 and 2007, respectively. In 2009, he was accepted as a Ph.D. student of Thermal Fluid Engineering in Yazd University. His research interests include fluid mechanics, CFD, aerodynamics and heat transfer.